



Parametric Study on Effect of Adding Stiffener to Post-tensioned Steel Connection

M. R. Shiravand¹ · A. Torabipour² · S. Mahboubi¹

Received: 3 November 2017 / Accepted: 30 July 2018 / Published online: 3 August 2018
© Korean Society of Steel Construction 2018

Abstract

Beam-to-column connections with post-tensioned (PT) elements are used in steel moment-resisting frames to provide adequate stiffness, strength, and ductility and to eliminate residual displacements under seismic loads. A steel PT connection has recently been developed with top and seat angles. In this connection, angles are used to dissipate energy under cyclic loading. This paper aims to investigate the influence of adding stiffeners to the top and seat angles on the cyclic responses of PT connections. To this end, a parametric study is performed to compare the effectiveness of stiffeners and some design parameters in the cyclic behavior of the PT connections. The design parameters are the angle thickness, the distance between the bolt line passing through the column and the heel of the angle (g_2), the PT force of the strands, and number of strands. First, the results of finite element analyses are compared to previously conducted experiments on PT connections with top and seat angles through a verification study. In this way, finite element models of 23 PT connections are developed and analyzed under cyclic loading. Results indicate that adding the stiffeners to the angles, enhances the energy dissipation capacity, moment capacity, stiffness and ductility of the PT connection much higher than improving other design parameters.

Keywords Post-tensioned connection · Self-centering moment-resisting frame · Stiffeners · Energy dissipation · Ductility

1 Introduction

Extensive damages to beam-to-column connections of steel moment-resisting frames during the 1994 Northridge and 1995 Kobe earthquakes, lead researchers to perform many efforts to improve the seismic performance of steel connections. As an alternative to bolted connections, a post-tensioned (PT) connection with top and seat angles was developed by Ricles et al. (2001, 2002) PT connections utilize high-strength steel strands in combination with bolted top and seat angles. The strands are anchored at the ends of beam against column and provide self-centering in the moment-resisting frames, while top and seat angles and the beam-to-column interface tolerate the transverse beam shear. The cyclic behavior of PT connections is characterized by the quantification of opening and closing of a gap

at the beam–column interface. The connection behavior is similar to a rigid connection until decompression occurs. Decompression is the process of releasing compression in the beam flanges. After decompression, the horizontal gap at the beam–column interface opens. A properly designed PT connection exhibits sufficient strength, stiffness, and ductility under earthquake excitations. Moreover, seismic damage is limited to top and seat angles that are replaceable, while beams and columns remain elastic. Ricles et al. (2001, 2002) and Garlock et al. (2005, 2007) performed a wide range of experimental and parametric studies on the cyclic behavior of PT connections and evaluated the effects of design parameters such as the connection strength and angle dimension on energy dissipation capacity and seismic behavior of the connection. Moreover, Garlock et al. (2005) studied cyclic behavior of six PT connections to examine the effect of initial PT force and number of PT strands on the seismic responses of PT connections. The authors concluded that PT connections show high ductility and energy dissipation capacity at 4% drift. In another study, Garlock et al. (2007) experimentally investigated the influence of the angle size on the stiffness, strength, and energy dissipation capacity of PT connections. The results show that the

✉ M. R. Shiravand
m_shiravand@sbu.ac.ir

¹ Department of Civil Engineering, Shahid Beheshti University, Tehran, Iran

² Department of Civil Engineering, Qazvin Azad University, Qazvin, Iran

angles exhibit considerable strength after yielding. Wolski et al. (2009) conducted some experiments to evaluate the combination of the PT connections with top and seat angles and PT strands. The results show that the PT force of the strands concentrates inelastic deformation on top and seat angles and eliminates residual drifts. Herning et al. (2011) analyzed three steel self-centering moment-resisting frames (SC-MRF) with PT connections under earthquake records to investigate the effect of geometric and structural properties on the seismic performance of SC-MRFs. Vasdravellis et al. (2013a) proposed a new self-centering PT connection that consists of the high-strength steel post-tensioned bars to provide self-centering behavior and steel cylindrical pins with hourglass shape which act as energy dissipation elements. The authors validated the connection behavior under quasi-static cyclic loading. In another study, Vasdravellis et al. (2013b) presented finite element models of the proposed PT connection with cylindrical pins with hourglass shape and calibrated the model with experimental tests. Moreover, they studied the effect of beam reinforcing, beam and column section sizes on the PT connection behavior through finite element analysis. Annan and Chiza (2013) characterized the resistance of slip-critical bolted joints with zinc-based metallized faying surfaces.

Moradi and Alam (2015) developed three-dimensional finite element models of PT connections with top and seat angles and validated the cyclic behavior of PT connections in finite element simulation against experiment results. Zhang et al. (2016) proposed a prefabricated PT self-centering beam-to-column connection with a bolted web friction device and tested seismic behavior of eight specimens of the connection was tested through experiments. Moradi and Alam (2017) performed a parametric study on the PT connection and concluded that beam depth and column height have a large impact on the initial stiffness, residual stiffness, and load capacity of the PT connection.

Shiravand and Mahboubi (2016) suggested adding the stiffeners to the top and seat angles of the PT connection, instead of increasing the thickness of the angle to improve cyclic behavior of the connection. The authors investigated the effect of adding stiffeners to top and seat angles on energy dissipation capacity of PT connections through numerical analyses and proposed some parametric relations to evaluate the cyclic behavior of PT connections with stiffened angles. Deformation of a decompressed PT connection with stiffened angle, introduced by Shiravand and Mahboubi (2016) is shown in Fig. 1. As observed, the mechanism of the cyclic behavior of the PT connection with stiffened angles is similar to the typical PT connection without stiffeners. The cyclic behavior of the connection is characterized by the quantification of opening and closing of a gap at the beam–column interface. The value of gap opening is defined as Δ_{gap} , as shown in Fig. 1, and the relative rotation

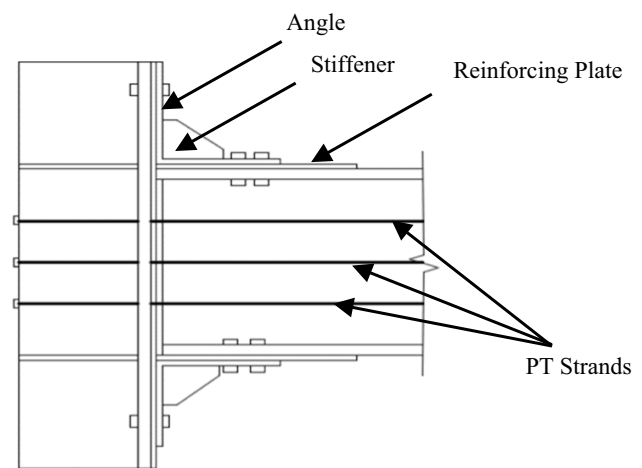


Fig. 1 PT connection with stiffened angles. Reproduced with permission from Shiravand and Mahboubi (2016)

between the beam and column is shown by θ_r . The connection behavior is similar to a rigid connection until decompression occurs, decompression is the process of releasing compression in the beam flanges. After decompression, the horizontal gap at the beam–column interface opens. Within these behavior the damage is concentrated in the stiffeners of the angles, while beams and columns remain elastic. According to Shiravand and Mahboubi (2016) study, in the PT connection with stiffened angles, the stiffeners delay the decompression and gap opening occurs at higher moment. The authors concluded that adding stiffeners to the angles results in increasing the energy dissipation capacity of the connection and concentrates the higher amount of residual defamiation in the angles.

Previous works show that in the PT connection with top and seat angles, the angles are the energy dissipation elements and their geometry affects significantly on the energy dissipation capacity of the connection. Furthermore, the most important advantage of top and seat angles is that they can be replaced after earthquake excitements. In the other hand, Shiravand and Mahboubi (2016) suggested that adding stiffeners can be an alternative to varying the angle geometry to improve energy dissipation capacity of the PT connection. The novelty in the proposed connection consists the use of stiffeners in top and seat angle to enhance the energy dissipation capacity of the PT connection and to simplify repair process. Considering the fact that, in addition to the energy dissipation capacity, other characteristics of PT connection may be influenced by stiffeners (for example: stiffness, moment capacity and...), further studies are required to determine the effectiveness of adding stiffeners, compared to other design parameters such as the angle geometry, the distance between the bolt line passing through the column and the heel of the angle (g_2) (on the stiffness, moment capacity,

ductility and energy dissipation capacity of PT connections. Hence, the present study aims to compare the effects of adding stiffeners to angles of the PT connection with the effects of some design parameters on the cyclic behavior of PT connections using finite element simulation. The design parameters are the angle thickness, the distance between the bolt line passing through the column and the heel of the angle (g_2), the PT force of the strands, and number of strands. To this end, finite element models of 23 PT connections are developed in the ABAQUS software (2010). First, the results of the finite element models are validated against prior experiments. Following, the finite element analyses are performed and the moment capacity, energy dissipation capacity, the stiffness and ductility of the PT connection specimens are estimated.

2 Finite Elements Models

The finite element software ABAQUS (2010) is used to develop three-dimensional models of 23 PT connections. The connection setup is shown in Fig. 2. The models consist of the beam, the column, angles, stiffeners, reinforcing plates, shim plates, PT strands, bolts, and anchorage plates. All the PT models have W36 × 150-wide flange beams and W14 × 398-wide flange columns. The column is 3962 mm high and the beam span is 4297 mm. The angles section for all models is L203 × 203 × 19.05, with a length of 406 mm. Two rows of bolts (two bolts) connect the angle to the beam flange and one row of bolts (four bolts) fastens the angle to the column flange. The bolts are A490 with 32 mm diameter. Each PT strand has a cross-sectional area of 140 mm². The thickness of the reinforcing plates and the continuity plates is 25 mm. The length of reinforcing plates of the beam flange is 1372 mm. Shim plates of size 406 × 292 × 32 mm

are placed between the angles and the beam flanges and column. The properties of the 23 PT models are presented in Table 1, where T_0 is total initial post-tensioning force, N_s is number of PT strands, g_2 is the distance between the bolt line passing through the column and the heel of the angle and L_0 is the length of stiffeners extension from the edge of the angle as shown in Fig. 3, and t_a is the thickness of angles. As observed, SP01 to SP07 are considered without stiffeners, while the specimens SP08 to SP13 are defined with stiffeners. The thickness of angles is taken different in specimens SP01, SP02, SP03 and SP04 and the three specimens SP05, SP06, and SP07 are modeled with different values of g_2 . Moreover, three different shapes of stiffeners—trapezoidal, triangular, and circular—are used in specimens with stiffened angles (SP08 to SP16). The values of T_0 and N_s are changed in SP17 to SP20 and SP21 to SP23 respectively.

Eight-node solid elements with reduced integral (C3D8R) is used for modeling the main components of connections including the beam, column, angles, reinforced plate, bolt, and shim plate. Solid elements can simulate plasticity, hyperelasticity, stress-stiffening, creep, large deflection, and large strain. To simulate the strands, the beam element (B31) is selected. The fine meshes are generated near the panel zone, with the expectation of plastic behavior. Figure 4 illustrates the meshing of the assembled model. Since the connection geometry is symmetric, only half of the connection is modeled in order to simplify the analyses and decrease the analyses operation. The properties of the materials are defined in accordance with the ASTM standards (1991) (Table 2). The modulus of elasticity of steel materials is considered to be 200 GPa and a bilinear stress–strain relationship is considered for all steel elements of PT models (Fig. 5). To define the bilinear stress–strain curve, the yield stress, the strain hardening, and the ultimate stress should be determined. The strain hardening (α) for the PT strands and bolts

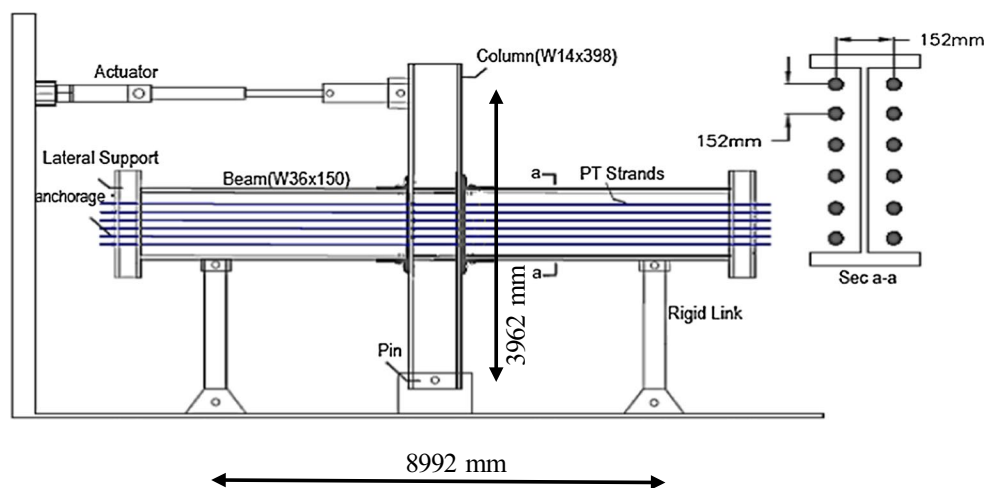
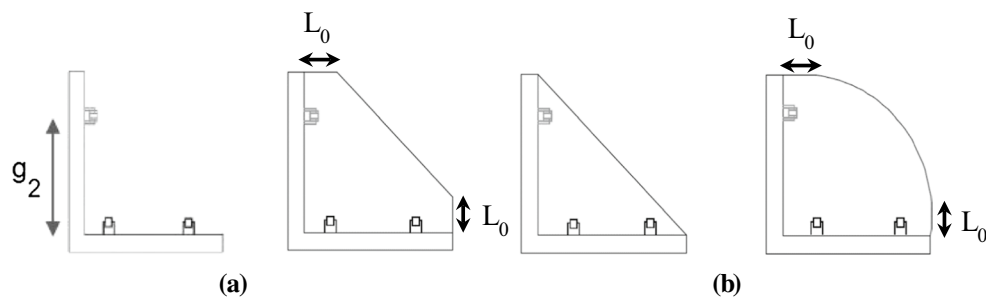


Fig. 2 General setup of PT connection in finite element simulation. Reproduced with permission from Garlock et al. (2005)

Table 1 Properties of specimens

Sample model	T_0 (kN)	N_s	g_2 (mm)	Stiffener shape	Stiffener (mm)	L_0 (mm)	t_a (mm)
SP01	3123	36	137	–	–	–	17.5
SP02	3123	36	137	–	–	–	19.05
SP03	3123	36	137	–	–	–	22
SP04	3123	36	137	–	–	–	25.5
SP05	3123	36	95	–	–	–	19.05
SP06	3123	36	127	–	–	–	19.05
SP07	3123	36	150	–	–	–	19.05
SP08	3123	36	137	Trapezoidal PL	183.95 × 183.95 × 20	23	19.05
SP09	3123	36	137	Trapezoidal PL	183.95 × 183.95 × 20	46	19.05
SP10	3123	36	137	Trapezoidal PL	183.95 × 183.95 × 20	65	19.05
SP11	3123	36	137	Triangular PL	101.95 × 101.95 × 20	–	19.05
SP12	3123	36	137	Triangular PL	117.95 × 117.95 × 20	–	19.05
SP13	3123	36	137	Triangular PL	183.95 × 183.95 × 20	–	19.05
SP14	3123	36	137	Circular PL	183.95 × 183.95 × 20	23	19.05
SP15	3123	36	137	Circular PL	183.95 × 183.95 × 20	46	19.05
SP16	3123	36	137	Circular PL	183.95 × 183.95 × 20	65	19.05
SP17	4059.9	36	137	–	–	–	19.05
SP18	3435	36	137	–	–	–	19.05
SP19	2810.7	36	137	–	–	–	19.05
SP20	2186.1	36	137	–	–	–	19.05
SP21	0	0	137	–	–	–	19.05
SP22	3123	24	137	–	–	–	19.05
SP23	3123	48	137	–	–	–	19.05

**Fig. 3** a Length of g_2 in specimens and b shapes of stiffeners used in SP08 to SP16 specimens

is assumed to be 0.05 and for other components, it is taken as 0.02. According to the axial force–displacement curve of strands, yield stress of the strand is equal to 85% of its ultimate stress. The tensile capacity, young modulus, and coefficient of thermal expansion of PT strands are 266 kN, 199 GPa, and $12e^{-6}$ respectively (ASTM 1997).

The interactions between the main components of the structures in contact with each other have a great influence on the precision of the nonlinear analyses. Therefore, the interactions between the other non-welded components are defined in two tangential and vertical directions. In the vertical direction, the interaction is determined as HARD CONTACT to avoid the penetration of the components into

each other. In the tangential direction, friction and frictionless contacts are defined. The frictionless contact is used to simulate the contact between the bolts and the strands with the hole and the nut with the angle, the beam, and the column. The contact between the angles with the reinforcing plates is determined by the friction contact. The friction coefficient for steel surfaces is considered 0.33 according to the ASTM (1991, 1997).

The column has pinned support to be allowed to rotate, and roller support is considered for the beam. The strands are firm at the ends of beam against the column. To establish symmetry conditions in finite element modeling, the movements of all points on the symmetry plane are limited to a direction

Fig. 4 Finite element model of PT connection with top and seat angle

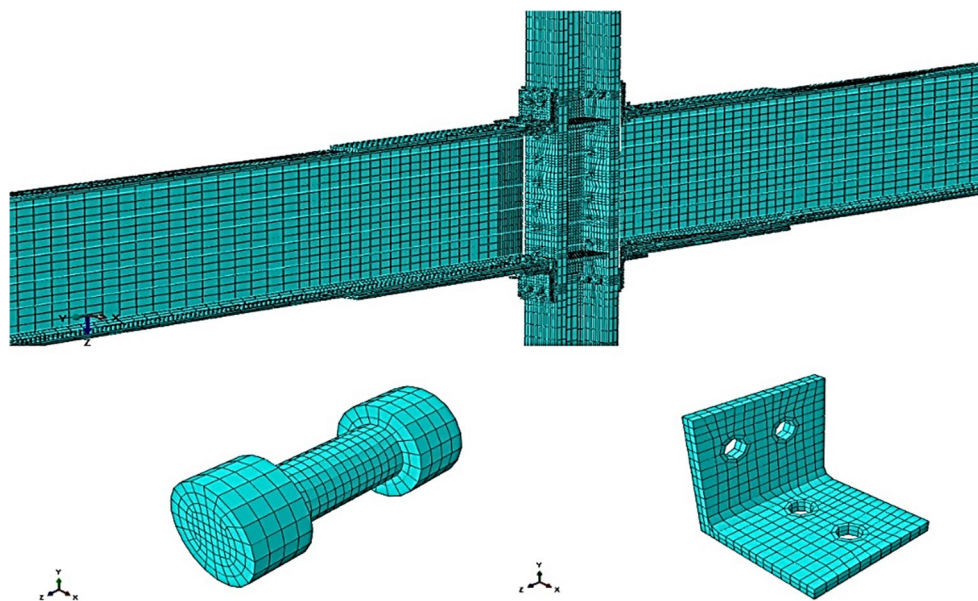


Table 2 Material properties. Reproduced with permission from Garlock et al. (2005)

Element	Beam flange	Beam web	Reinforcing and shim plate	Column flange	Column web	Angle	Strands	Stiffener	Bolt
Yield stress (MPa)	362	414	397	356	345	383	1620	345	800
Ultimate stress (MPa)	498	527	574	499	496	545	1900	496	1000

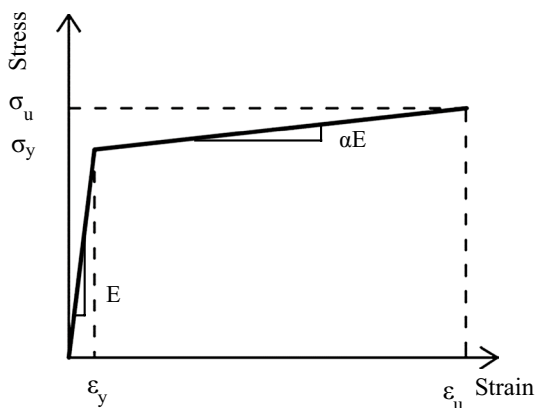


Fig. 5 Bilinear stress–strain behavior of steel materials

perpendicular to the plane, the rotation of the points is limited around the two axes on the symmetry plane. The displacement

cyclic loads are applied on PT connection models according to the SAC-loading protocol (Table 3) (Venture 1997).

In order to investigate the behavior of the PT connections under cyclic loading, nonlinear analyses are performed. Prior to applying the cyclic loads, the initial condition of the models includes pretension forces of the PT strands and the bolts are assigned. Following this, the cyclic loading is applied in terms of several displacement load steps and nonlinear static analyses are performed considering the geometric and material nonlinearity and large deformation effects. It is assumed that the load steps are small and loads are applied slowly on the top the PT connections column.

3 Verification Study

According to the efforts by Moradi and Alam (2015) and Shiravand and Mahboubi (2016), finite element analyses of the PT connections provide reliable and accurate results. In this study, in order to verify the finite element analyses results, the finite

Table 3 Cyclic loading protocol. Reproduced with permission from Venture (1997)

Load step	1	2	3	4	5	6	7	8
Number of cycles	0.00375	0.005	0.0075	0.01	0.015	0.02	0.03	0.04
θ (rad)	0.005	6	6	4	2	2	2	2

element models of four PT connections previously tested by Garlock et al. (2005) and two PT connections tested by Zhang et al. (2016) are developed. The material properties and the boundary condition of the finite element model are considered to be identical to the experiment (Garlock et al. 2005; Zhang et al. 2016). Figure 6 shows the Von Mises stress distribution in the finite element model of specimen 36s-20-P (Garlock et al. 2005). As observed, maximum tension is concentrated on the top and seat angles.

Comparison of the hysteresis behavior of the PT connection in the experimental (36s-20-P) and finite element analyses is shown in Fig. 7. As observed, there is a good agreement between finite element and experiment results. The obtained results of finite element analyses and experiment of all specimens (Garlock et al. 2005; Zhang et al. 2016) are presented in Table 4 and the error percent for each parameter is calculated. According to Table 4, the maximum error is 2.12%, which indicates that finite element simulation can provide precise response and predict the behavior of the PT connections accurately. In Table 4, T_0 is the initial post-tensioning force of strands, T_u is the ultimate force of all strands, T_{max} is the maximum post-tensioning force of the strands at 4% drift, M_d is the decompression moment, θ_{rmax}

is the maximum relative rotation at beam–column interface, and Δ_{gap} is amount of gap opening.

Figure 8 shows the gap opening mechanism at the beam-to-column interface. As seen the finite element could predict the behavior of the angles and the PT connection.

4 Finite Element Analyses and Results

Figure 9 shows the Von-Mises stress distribution of some connections as an example. As seen, damage is concentrated on the angles and the stiffeners of the PT connection. Noted that although partial yielding is observed in some small regions of beams but no damage occurs in the beams and the column.

Table 5 lists the responses of 23 specimens in finite element analyses. The response parameters in Table 5 are the maximum moment of the PT connection (M_{max}), the plastic moment capacity of the beam (M_p), the maximum post-tensioning force of strands (T_{max}), the ultimate strength of the PT strands (T_u), the maximum relative rotation at the beam–column interface (θ_{rmax}), and the value of gap opening (Δ_{gap}). The value of the M_p is considered to be 3282 kN m.

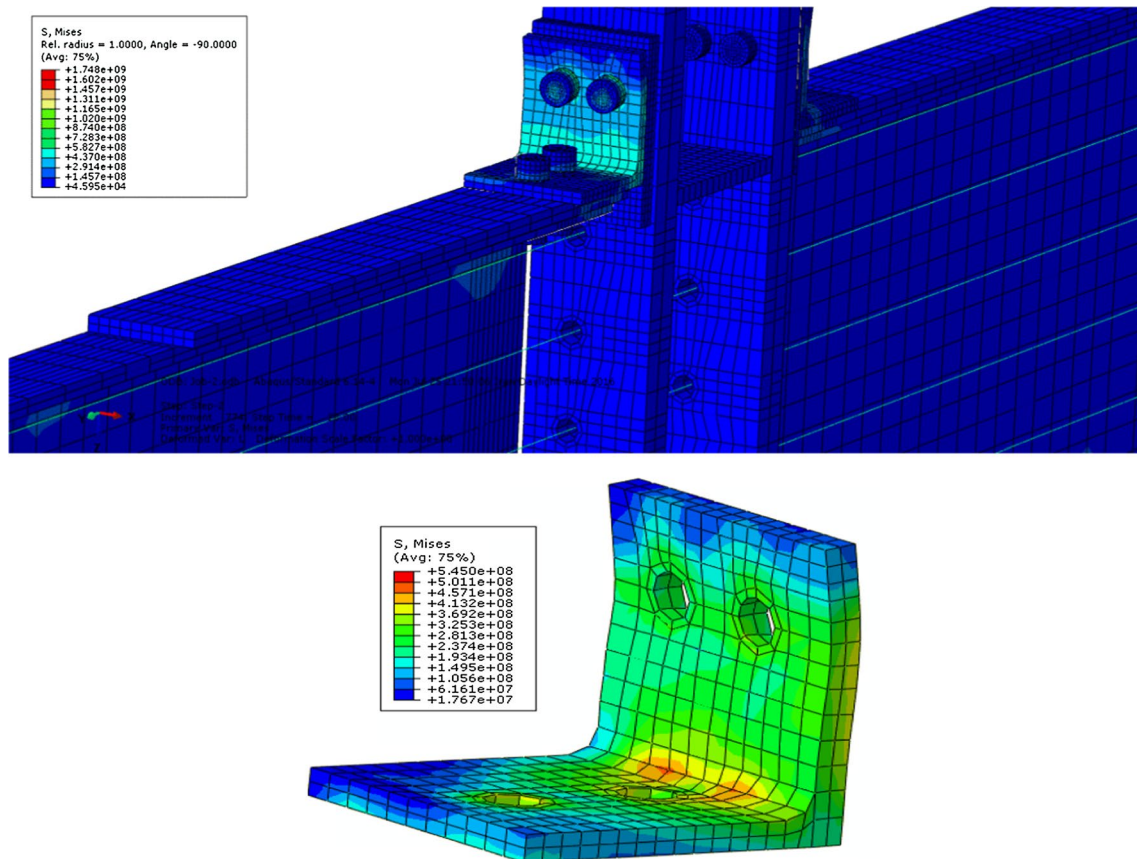


Fig. 6 Distribution of Von-Misses stress in verification model (specimen 36s-20-P) Reproduced with permission from Garlock et al. (2005)

Fig. 7 Comparison of hysteresis behavior of the PT connection in finite element and experiment) 36s-20-P) Reproduced with permission from Garlock et al. (2005)

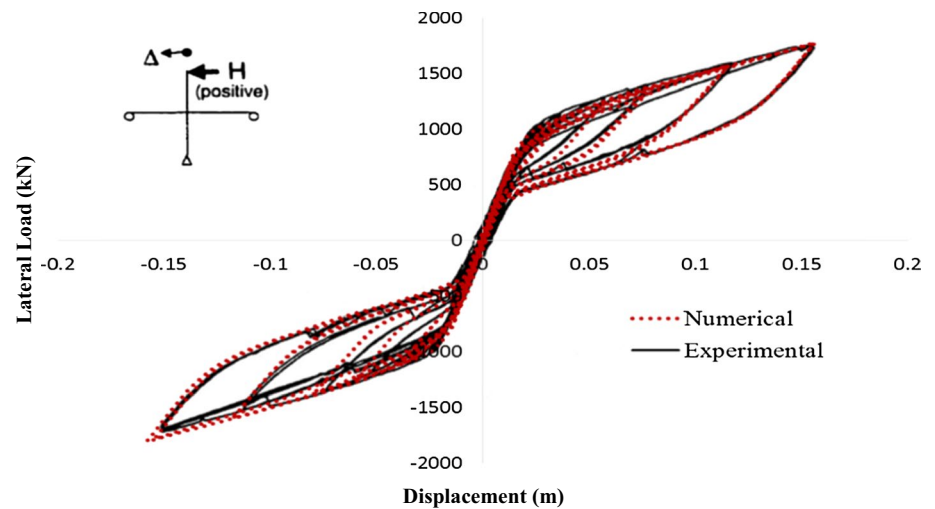


Table 4 Comparison of experimental and finite element results

Sample model	T_0 (kN)	θ_{max} (rad)	$\frac{M_d}{M_p}$	$\frac{T_{max}}{T_u}$	θ_{rmax} (rad)	References
(36s-20-P) _{EXP}	3194	4%	0.47	0.55	0.033	Garlock et al. (2005)
(36s-20-P) _{FE}	3123	4%	0.464	0.551	0.0332	
Error percent	2%	0	1.27%	0.18%	0.6%	
(36s-30-P) _{EXP}	4759	2%	0.65	0.58	0.013	Garlock et al. (2005)
(36s-30-P) _{FE}	4690.7	2%	0.631	0.582	0.0132	
Error percent	1.5%	0	2.1%	0.2%	1.5%	
(36s-30) _{EXP}	4728	1.7%	0.68	0.52	0.006	Garlock et al. (2005)
(36s-30) _{FE}	4643.8	1.7%	0.668	0.523	0.00612	
Error percent	1.7%	0	1.76%	0.5%	2%	
(16s-45) _{EXP}	3051	3.6%	0.47	0.86	0.029	Garlock et al. (2005)
(16s-45) _{FE}	3010	3.6%	0.46	0.863	0.0293	
Error percent	1.3%	0	2.12%	0.35%	1.03%	
PSCC1 _{EXP}	2055	3.5%	0.47	0.572	0.0237	Zhang et al. (2016)
PSCC1 _{FE}	2034.06	3.5%	0.461	0.57	0.0239	
Error percent	1.02%	0	1.9%	0.34%	0.84%	
PSCC2 _{EXP}	2566.9	3.5%	0.48	0.58	0.0212	Zhang et al. (2016)
PSCC2 _{FE}	2546	3.5%	0.474	0.576	0.0214	
Error percent	0.8%	0	1.25%	0.69%	0.94%	

The results show that thickness of the angle affects the gap opening and the relative rotation between beam and column of the PT connections. For connections with higher t_a (thickness of angle), lower values of Δ_{gap} and θ_{rmax} are obtained. As the thickness of the angle increases from 17.5 to 25.5 mm (SP01-SP04), the values of Δ_{gap} and θ_{rmax} decrease by 4.4% and 4.5%, respectively. Moreover, the connections with lower g_2 value exhibit a large gap opening and relative rotation. The PT connections with stiffened angles provide on average 30% greater moment capacity under cyclic loading and the maximum moment of the connection is observed in SP10.

According to Table 5, comparison of the moment capacity of the specimens shows that the increase in the

thickness of the angle from 19.05 mm to 25.5 mm (SP02 and SP04), increases the moment capacity of the connection around 17%, and decreasing the value of g_2 (the distance between the bolt line passing through the column and the heel of the angle), from 137 to 95 mm (SP02 and SP05), results in 10% greater moment capacity of the PT connection. Moreover, a 30% increase in the initial post-tensioning forces of the strands increases (SP17 and SP02), increases the moment capacity of the connection approximately 10%. When the number of post-tensioned strands increases from 36 to 48 (SP02 and SP23), the moment capacity of the connection improves by 9.5%. While investigation of moment capacity of specimens with stiffened angles (SP08–SP16) indicates that, adding the



Fig. 8 PT connection in **a** experimental analyses by Garlock et al. (2005) (36s-20-P). **b** Finite element analyses at 4% drift ratio

stiffeners to the connection SP02, enhances the moment capacity of the connection up to 40% (SP10).

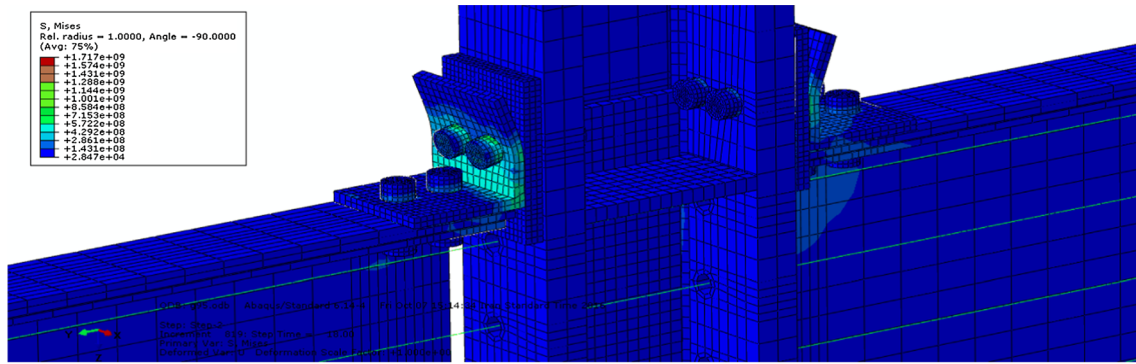
In order to investigate the effect of adding stiffeners, Fig. 10 compares the variations of the axial force in the PT strand versus drift ratio in the specimen without stiffeners (SP02) to the specimens with stiffeners (SP10 and SP13) under cyclic loading. As observed, the PT force of the strands in SP02 shows a greater loss compared to the PT forces of SP10 and SP13 under cyclic loading. Moreover, according to Table 5, the ratios of the maximum post-tensioning force of the strands to the ultimate strength of strands ($\frac{T_{\max}}{T_u}$) of specimens with stiffeners (SP10 and SP13) are 3.8% and 5.8% lower than that of the specimens without stiffener (SP02), respectively.

4.1 Effect of PT Strands and Stiffeners

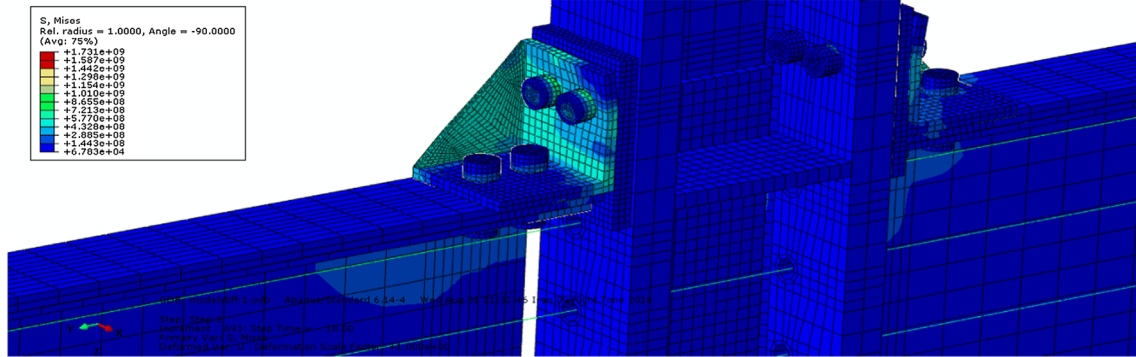
The angles and the strands are the main elements of the PT connection. Two angles and the friction at the beam–column interface tolerate the transverse shear, while the strands provide the flexural strength and restore the forces of the PT connection. To investigate the part of flexural strength provided by the strands and to achieve the amount of energy dissipated by the angle, the strands and the stiffeners, the specimen SP02 is analyzed under cyclic loading in four conditions; the PT connection with the top and seat angles and the PT strands (SP02), the PT connection without the angles (SP02-s), and the PT connection without the strands (SP02-a) and the PT connection with stiffened angles (SP13). It should be noted that SP02-a is similar to specimen SP21. All four specimens are subjected to cyclic loading up to 4% drift angle. The loading protocol proposed by AISC (2016)

for beam-to-column connection in intermediate, a special moment frame is used. The lateral force–displacement behavior of three specimens is compared in Fig. 11.

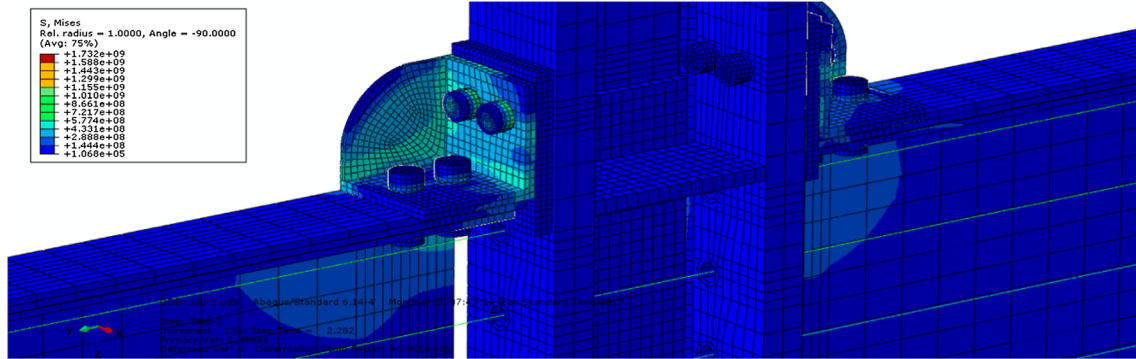
The area surrounded by hysteresis loops is defined as energy dissipation capacity. As seen, the area enclosed by hysteresis loops of the PT connection without strands (SP02-a) is approximately equals to that of the connection with the angle and strands (SP02), while for the PT connection without angles (SP02-s), the area of the hysteresis loops is negligible. Therefore, the energy dissipation capacity of the PT connection with angles and without the strands is equal to the PT connection with the angles and the strands. This confirms that the angles dissipate the total energy of the PT connection under cyclic loading, while the strands remain elastic during loading. As seen, the general response of SP02 (the PT connection with angles and strands) is due to the incorporation of the non-linear elastic contribution from PT strands (SP02-s) and elasto-plastic hysteresis response of the angle (SP02-a). Moreover, as observed, the area surrounded by the hysteresis loop of specimen with stiffeners (SP13) is larger than the specimen without stiffeners (SP02), which indicates that adding the stiffeners increases the energy dissipation capacity of the PT connection. The ratio of the flexural moment and the post-yield stiffness (K_{py}) of SP02-s, SP02-a and SP13 to those of SP02, are presented in Table 6. As observed, the ratios of the maximum moment to the plastic moment capacity of the beam in SP02-s and SP02-a are 73% and 32% respectively, which indicates that most of the moment capacity of the PT connection is provided by the strands. Moreover, 69% of the maximum moment of the PT connection is provided by the strands, while the angles proportion in the flexural strength is 31%. In



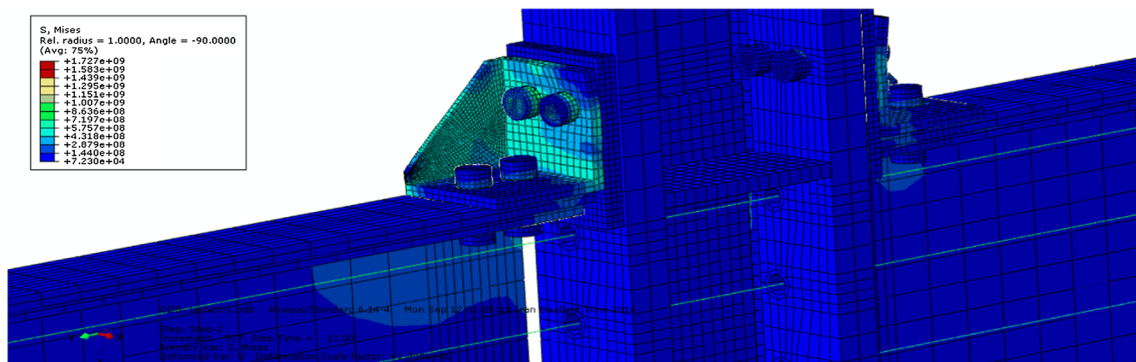
SP05



SP10



SP13

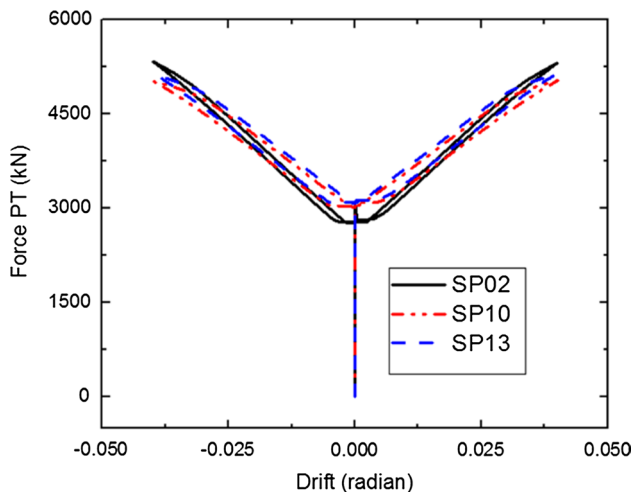


SP16

Fig. 9 Von-Mises stress distribution in the connection components

Table 5 Response of specimens in finite element analyses

Sample model	$\frac{M_{max}}{M_p}$	$\frac{T_{max}}{T_u}$	θ_{rmax} (mm)	Δ_{gap} (mm)
SP01	1.02	0.54	0.0334	29.5
SP02	1.05	0.55	0.0325	28.71
SP03	1.17	0.53	0.0322	28.5
SP04	1.23	0.53	0.0319	28.2
SP05	1.16	0.54	0.0330	29.2
SP06	1.02	0.54	0.0328	29
SP07	0.99	0.54	0.0320	28.3
SP08	1.25	0.52	0.0314	27.8
SP09	1.27	0.52	0.0322	28.40
SP10	1.48	0.52	0.0321	28.47
SP11	1.1	0.53	0.0325	28.74
SP12	1.13	0.54	0.0329	29.14
SP13	1.22	0.53	0.0322	28.42
SP14	1.24	0.51	0.0313	27.5
SP15	1.26	0.52	0.0312	27.61
SP16	1.28	0.52	0.0311	27.63
SP17	1.16	0.61	0.0324	28.6
SP18	1.1	0.56	0.0332	29.3
SP19	1.03	0.51	0.0342	30.2
SP20	0.96	0.45	0.0347	30.7
SP21	0.32	0	0.0434	38.3
SP22	0.82	0.57	0.0358	31.6
SP23	1.15	0.49	0.0314	27.7

**Fig. 10** PT forces versus drift for SP02, SP10 and SP13

addition, as presented in Table 6, the elastic stiffness of the strands provides 68% of the post-yield stiffness of the PT connection, while around 32% of the post-yield stiffness is a result of the plastic stiffness of the angle. In the other hand, the ratio of the post-yield stiffness of the PT connection with stiffened angles (SP13) to that of the connection without stiffeners (SP02) is 1.092, which indicates

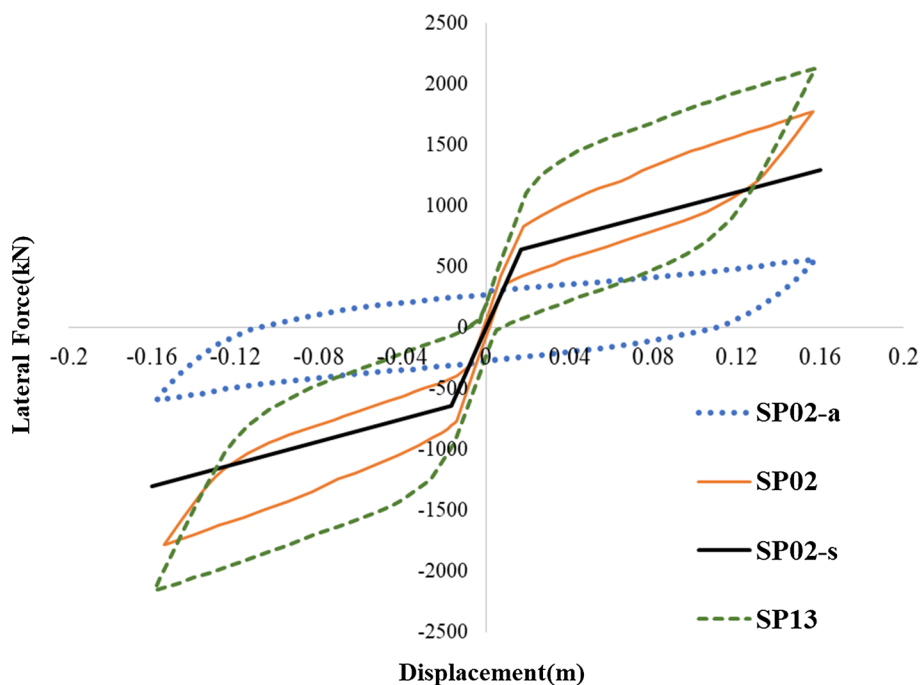
that adding the stiffeners improves the post-yield stiffness of the PT connection by 9.2%.

Moreover, comparison of the results of SP17 to SP20 (Table 5) shows that a decrease in the initial post-tensioning forces of the strands decreases the plastic moment capacity and the maximum post-tensioning forces of the PT connection. As the value of T_0 decreases from 3435 (SP17) to 2186 (SP20), the relative rotation ($\theta_{r,max}$) and the gap opening (Δ_{gap}) increase by 5.5% and 7.3%, respectively. Furthermore, the results of SP21, SP22, and SP23 (Table 5) illustrate that the increase in number of the strands improves the plastic moment capacity of the PT connection and decreases the values of $\theta_{r,max}$ and Δ_{gap} . Moreover, according to the ratio of the maximum moment to the plastic moment capacity of SP20 (Table 5) and SP02-a (Table 6), the plastic moment capacity of the connection without the strands decreases up to 60%.

4.2 Moment-Relative Rotation Curves

The moment–relative rotation ($M-\theta_r$) hysteresis curves of some specimens are presented in Fig. 11. As seen, all the specimens reach the relative rotation of 0.03 rad. Comparison of the hysteresis behavior of SP01 to that of SP04 shows that the increase in the thickness of the angles increases the moment capacity of the connections. The maximum moment of SP04 during cyclic loading is around 4000 kN m, while SP01 reaches the maximum moment of 3347 kN m. Moreover, the hysteresis behavior of SP05, SP06, and SP07 shows the PT connections. As g_2 value increases, the moment capacity of the connection decreases; for example, for SP05 with g_2 value of 95 mm, the connection reaches a moment value of 3807 kN m, while for SP06 and SP07, in which g_2 values are 127 mm and 150 mm respectively, the maximum moments of the connections under cyclic loading are 3350 kN m and 3249 kN m, respectively. According to Fig. 12, the hysteresis behavior of SP08–SP16 shows that the PT connections with stiffened angles have larger load-carrying capacity and the stiffeners increase the maximum moment capacity of the PT connections. For example the maximum moment capacity of the PT connections with stiffeners reaches 4860 kN m (SP10) which is 40% higher than similar specimen without stiffeners (SP02). While increasing the angle thickness and decreasing the g_2 (the distance between the bolt line passing through the column and the heel of the angle) of the specimen SP02, enhances the moment capacity of the connection 17% and 10%. Hence, adding stiffeners exhibit higher effects on improving the moment capacity of the PT connection. Moreover, the larger amount of L_0 in trapezoidal stiffeners (SP08–SP10) enhances the moment capacity of the PT connection. As the size of stiffeners increases in the connections with triangular stiffeners (SP11–SP13), the moment capacity of the connection increases.

Fig. 11 Lateral force–displacement behavior of SP01, SP01-s, SP01-a and SP13



4.3 Energy Dissipation Capacity

Energy dissipation is the area enclosed by the hysteresis loops. SP02 is taken as the control specimen and the energy dissipation capacity of the specimens is compared to SP02 in Fig. 13. As observed in Fig. 13a, the energy dissipation capacity of SP01 is lower than that of SP02, SP03, and SP04. These four connections have the same properties, but the thickness of angle is different. The results indicate that the increase in the thickness of angle increases the energy dissipation capacity of the PT connection. As the thickness of the angle increases from 17.5 mm to 25.5 mm, the energy dissipation capacity of the connection increases up to 42%. Figure 13b compares the energy dissipation capacity of SP05, SP06, and SP07 to SP02, which have the same angle size but different g_2 values (the distance between the bolt line passing through the column and the heel of the angle). As seen, the specimen with smaller g_2 (SP05) exhibits a higher amount of energy dissipation and the increase in g_2 results in decreasing the energy dissipation capacity of the

connection. As observed in Fig. 13 c, d, e, adding stiffeners to the angles of the PT connections improves the energy dissipation capacity of the connection. The trapezoidal, triangular, and circular stiffeners increase the energy dissipation capacity of the PT connection by 80, 72, and 86%, respectively. As observed the PT connections with circular stiffeners exhibit higher energy dissipation capacity compared to those with trapezoidal and triangular stiffeners. For the specimen with trapezoidal stiffeners (SP08, SP09 and SP10), the increase in the value of L_0 enhances the energy dissipation capacity of the connection. On the other hand, for specimen with circular stiffeners (SP14, SP15 and SP16), as the value of L_0 increases, the energy dissipation capacity of the connection decreases. In SP11–SP13, which have triangular stiffeners, the amount of energy dissipation increases by 34% as the size of stiffeners increases.

Table 6 comparison of moment and post yield stiffness of SP02, SP02-s, SP02-a and SP13

Sample model	$\frac{M_{max}}{M_p}$	$\frac{M_{max}}{M_{SP02}}$	K_{py} (kN/m)	$\frac{K_{py}}{K_{py(SP02)}}$
SP13	1.22	1.16	581	1.092
SP02	1.05	1	532	1
SP02-s	0.73	0.69	362	0.68
SP02-a	0.32	0.31	170	0.32

According to Fig. 13f, the decrease in initial post-tensioning forces of SP17–SP20 has a decreasing impact on energy dissipation capacity of the PT connection. As the initial post-tensioning force of strands decreases by 46%, the amount of the energy dissipation decreases from 725 kN m to 691 kN m. Moreover, as observed in Fig. 13g, an increase in the number of strands increases the energy dissipation capacity of the PT connection; as the number of strands increases from 0 to 48, the energy dissipation capacity of the PT connection increases by around 31%.

In addition, the effects of the design parameters on energy dissipation capacity of the PT connection can be compared to those of adding stiffeners. According to Fig. 13, the increase in thickness of the angle by 33% (SP02 and SP04), increases the energy dissipation capacity of the

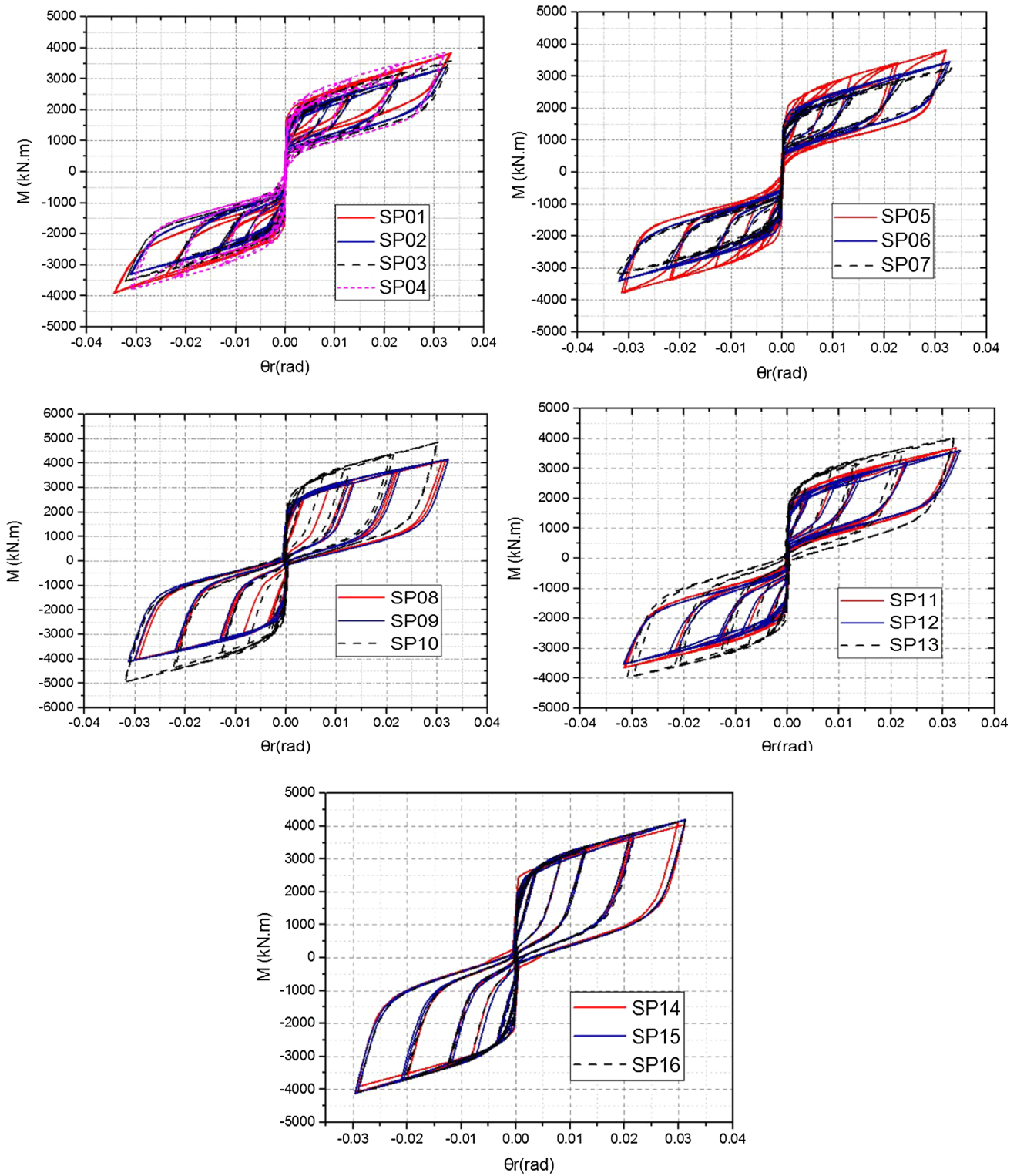


Fig. 12 Moment–relative rotation curves of specimens

PT connection approximately by 3%, and the decrease in the values of g_2 (the distance between the bolt line passing through the column and the heel of the angle), from

17 to 95 (SP02 and SP05) results in 20% increase in the energy dissipation capacity of the PT connection. A 33% greater number of PT strands (SP02 and SP17), improves the

energy dissipation capacity by 4.3% and a 30% larger initial post-tensioning forces of strands (SP02 and SP17) provides 2.8% higher energy dissipation capacity. While adding stiffeners to the specimen SP02, enhances the energy dissipation capacity of the PT connection up to 85%.

4.4 Effect of Multi-parameters

In order to study the effects of the thickness of the angles and the thickness of the stiffeners on behavior of the PT connection under cyclic loading, some additional analyses are performed and the energy dissipation capacity, the initial stiffness, and moment capacity of some specimens varying the thickness of the angle and the stiffeners are estimated. Figure 14 shows the variation of the energy dissipation capacity (E_d), initial stiffness (K_i) and the moment capacity ratio ($\frac{M_{max}}{M_p}$) of the PT connection under the simultaneous

effects of the thickness of the angle (t_a), the thickness of the stiffeners (t_s) and g_2 (the distance between the bolt line passing through the column and the heel of the angle) by contour plots. Each plot consists of two horizontal axis that indicate the control variables and a vertical axis that shows the response parameter. For example in Fig. 14a, for t_a and g_2 value of 20 mm and 140 mm, respectively, the amount of energy dissipation capacity of the connection locates on yellow contour. Figure 13a, b show a 3D plot of the energy dissipation capacity under the effect of g_2 , the thickness of the angle (t_a), and the stiffeners (t_s). As observed, the increase in the thickness of the angle and the stiffeners results in a higher energy dissipation capacity of the PT connection, while the g_2 value has a decreasing effect on the energy dissipation capacity of the PT connection. For example, as t_a increases from 18 mm to 22 mm, for g_2 (the distance between the bolt line passing through the column and the heel of the angle) of 148 mm, the energy dissipation capacity of the PT connection is predicted to increase up to 10%. The increase in the thickness of the stiffeners from low level to high level (10 mm to 20 mm) increases the energy dissipation capacity of the PT connection by 25%. Moreover, when the g_2 value increases from 128 mm (low level) to 148 mm (high level) for a constant value of the angle thickness (19 mm), the energy dissipation capacity of the PT connection decreases by 14%. As observed, the maximum energy dissipation of the PT connection can be achieved when the g_2 is at a lower level and t_a is at a higher level ($g_2 = 128$ mm and $t_a = 22$ mm). Figure 14c, d show the effects of t_a , t_s , and g_2 on the initial stiffness of the PT connection in a 3D plot. As observed, the thickness of the angle and the stiffeners exhibit an increasing impact, while the g_2 value has a decreasing effect on the initial stiffness of the PT connection. The maximum amount of initial stiffness can be achieved in the lower level of thickness and the higher level

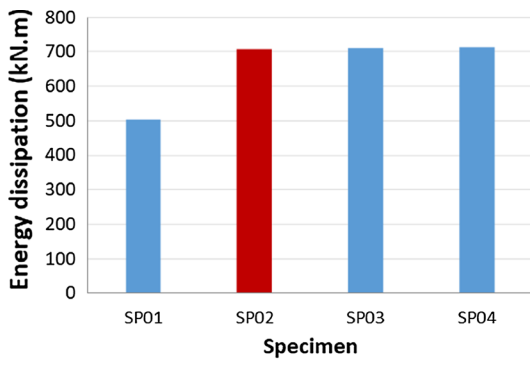
of g_2 . Moreover, the effects of these factors are considerable on the energy dissipation capacity of the connection compared to the initial stiffness. As the t_a and t_s increase from low level to high level, the initial stiffness of the PT connection increases up to 0.85%. The effects of t_a , t_s , and g_2 on the flexural moment capacity of the PT connection are illustrated in Fig. 14e, f. As seen, the thickness of the angles and the stiffeners has an increasing impact on the moment capacity of the connection. As the values of t_a and t_s increase from minimum to maximum, the moment capacity of the PT connection increases by 3% and 8%, respectively. Moreover, g_2 value exhibits a decreasing effect on the moment capacity of the PT connection. According to Fig. 14d, f, the PT connection reaches the maximum moment capacity when the t_a , t_s , and g_2 are 22 mm, 20 mm, and 130 mm respectively.

4.5 Effect of Stiffeners on Stiffness of PT Connections

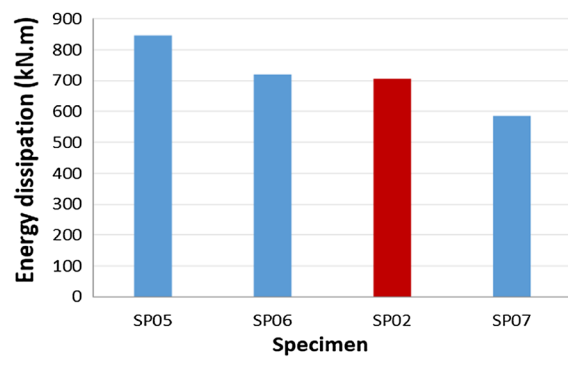
The secant stiffness of the PT connection specimens is calculated using moment–rotation responses of the connection according to AISC (2016). In order to study the effects of design parameters and stiffeners on the stiffness of the PT connection, the ratios of secant stiffness of specimens to that of SP02 ($\frac{K_{s_{spn}}}{K_{s_{sp02}}}$) is presented in Table 7. As seen, the secant stiffness of SP04 is 1.0178 times larger than the secant stiffness of SP02, which indicates that a 33% increase in the thickness of the angle increases the stiffness of the PT connection by 1.78%. Moreover, the decrease in the values of g_2 (the distance between the bolt line passing through the column and the heel of the angle), by 30% (SP05), exhibits a negligible effect on the secant stiffness of the connection and increases the secant stiffness of the PT connection by 0.8%. According to Table 7, the PT connections with stiffened angles exhibits higher stiffness and the secant stiffness of the connection with stiffeners is on average 3% larger than that of the connection without stiffeners (SP02). In addition, adding the stiffeners to the angles of the PT connections can improve the secant stiffness of the connection up to 3.68% (SP16).

Moreover, the initial post-tensioning forces strands shows an increasing effect on the secant the PT connection and the specimen with higher T_0 (SP17), provides 3.55% greater stiffness. Furthermore, a larger number of the PT strands can also increase the secant stiffness (SP23).

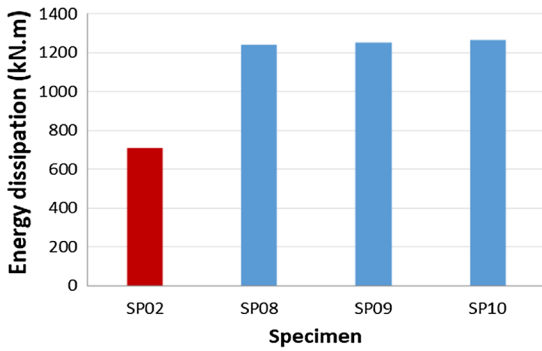
Ductility is of great importance in the seismic design of steel connections. Ductility is the ability of a connection to resist large inelastic deformation without significant degradation in strength and without occurrence of structural instability and collapse. Ductility can be quantified with the ductility index, which is the ratio of the ultimate rotation of the connection to the rotation corresponding to the connection



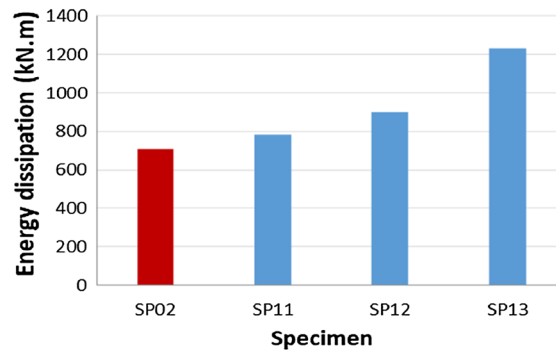
(a)



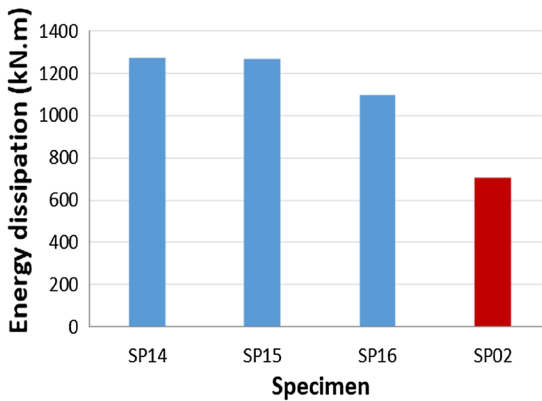
(b)



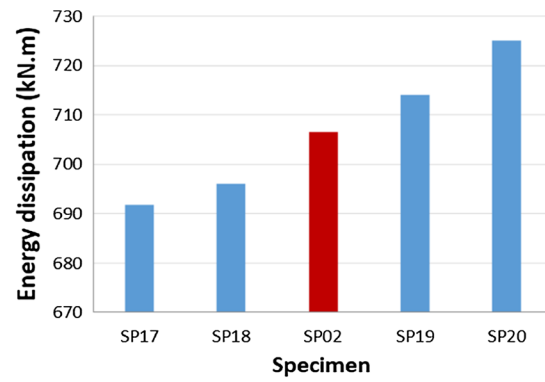
(c)



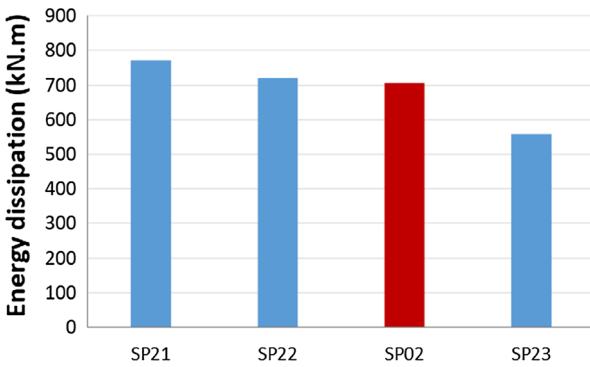
(d)



(e)



(f)



(g)

Fig. 13 Energy dissipation capacity of specimens. **a** Effect of angle thickness, **b** effect of g_2 , **c** effect of trapezoidal stiffeners, **d** effect of triangular stiffeners, **e** effect of circular stiffeners, **f** effect of initial PT force of strands

yielding ($\mu = \frac{\theta_u}{\theta_y}$). Following this, the values of θ_u and θ_y are calculated using the moment–relative rotation curves (Fig. 11), and ductility index (μ) is estimated for all the PT connection specimens. Table 8 shows the ductility index of all 23 specimens. As observed, SP10 exhibits maximum ductility under cyclic loading (2.76) while the minimum ductility factor is obtained for SP21 (1.3). Moreover, the results show that adding the stiffener to the top and seat angles of the PT connection increases the ductility of the PT connections. The average value of the ductility index for the PT connections with stiffeners (SP08–SP16) is 2.41, which is 32% greater than SP02. While increasing the thickness of the angle from 17.5 mm to 25.5 mm, improves the ductility of the connection by 16%. On the other hand, the increase in g_2 (the distance between the bolt line passing through the column and the heel of the angle) from 95 to 150 decreases the μ by 21%. Comparison of the ductility index of SP17 to that of SP20 indicates that by using a greater initial post-tensioning force, the ductility of connection can be enhanced by up to 45%. Furthermore, the PT connection, with larger number of strands (SP23) exhibits 77% higher ductility.

5 Summary and Conclusion

In this paper, the effects of adding stiffeners on the cyclic characteristic of PT connections are compared to the effects of four design parameters include; the angle thickness, the distance between the bolt line passing through the column and the heel of the angle (g_2), the PT force of the strands, and number of strands. Hence, finite element models of 23 PT connection specimens are developed and the moment–relative rotation, the energy dissipation capacity and the stiffness and ductility of the specimens are estimated through nonlinear analyses and compared to those of a control specimen. The results are summarized below:

- The results indicate that adding the stiffeners to the PT connection with top and seat angles provides much higher moment capacity in the PT connection under cyclic loading compared to the increase in the thickness of the angle, decreasing the values of g_2 (the distance between the bolt line passing through the column and the heel of the angle), the increase in the initial post-tension-

ing forces of the strands and numbers of the PT strands. The PT connections with stiffened angles provide a 40% greater moment capacity, while a 33% increase in the thickness of the angles, a 30% decrease in the values of g_2 , a 30% increase in initial post-tensioning forces of the strands and a 33% increase in number of PT strands enhances the moment capacity of the PT connection by 17%, 10%, 10% and 9.5%, respectively.

- The PT connections with stiffened angles exhibit higher post-yield stiffness approximately by 10% compared to the PT connection without stiffeners.
- Adding the stiffeners to the angles of the PT connection shows a considerable effect on energy dissipation capacity of the connection compared to improving other design parameters. A 33% increase in the thickness of the angle, improves the energy dissipation capacity of the PT connection approximately by 3%, the decrease in the values of g_2 (the distance between the bolt line passing through the column and the heel of the angle), by 30% results in a 20% higher energy dissipation capacity. In addition, a 33% greater number of PT strands enhances the energy dissipation capacity by 4.3% and a 30% larger initial post-tensioning forces of strands provides 2.8%, higher energy dissipation capacity. While adding stiffeners to the specimen SP02 enhances the energy dissipation capacity of the PT connection up to 85%.
- As the size of the stiffeners increases in the PT connection with triangular stiffeners, the influence of the stiffeners in improving the cyclic behavior of the PT connection increases. Using some larger triangular stiffeners, the load-carrying capacity and the energy dissipation enhances by 11% and 34% respectively. In addition, a larger L_0 in the PT connection with trapezoidal stiffeners provides 18% greater moment capacity.
- Adding the stiffeners to the angles results in higher stiffness of the connection compared to the increase in the thickness of the angles, decreasing the values of g_2 (the distance between the bolt line passing through the column and the heel of the angle), increasing the initial post-tensioning forces strands and number of PT strands. A 33% increase in the thickness of the angle increases the secant stiffness of the PT connection by 1.78%. The decrease in the values of g_2 , by 30%, increases the secant stiffness of the PT connection by 0.8%, the connection with higher T_0 provides 3.55% greater stiffness. While adding the stiffeners to the angles of the PT connections can improve the secant stiffness of the connection up to 3.68%.
- The results show that adding the stiffener to the top and seat angles of the PT connection increases the ductility of the PT connections. The average value of the ductil-

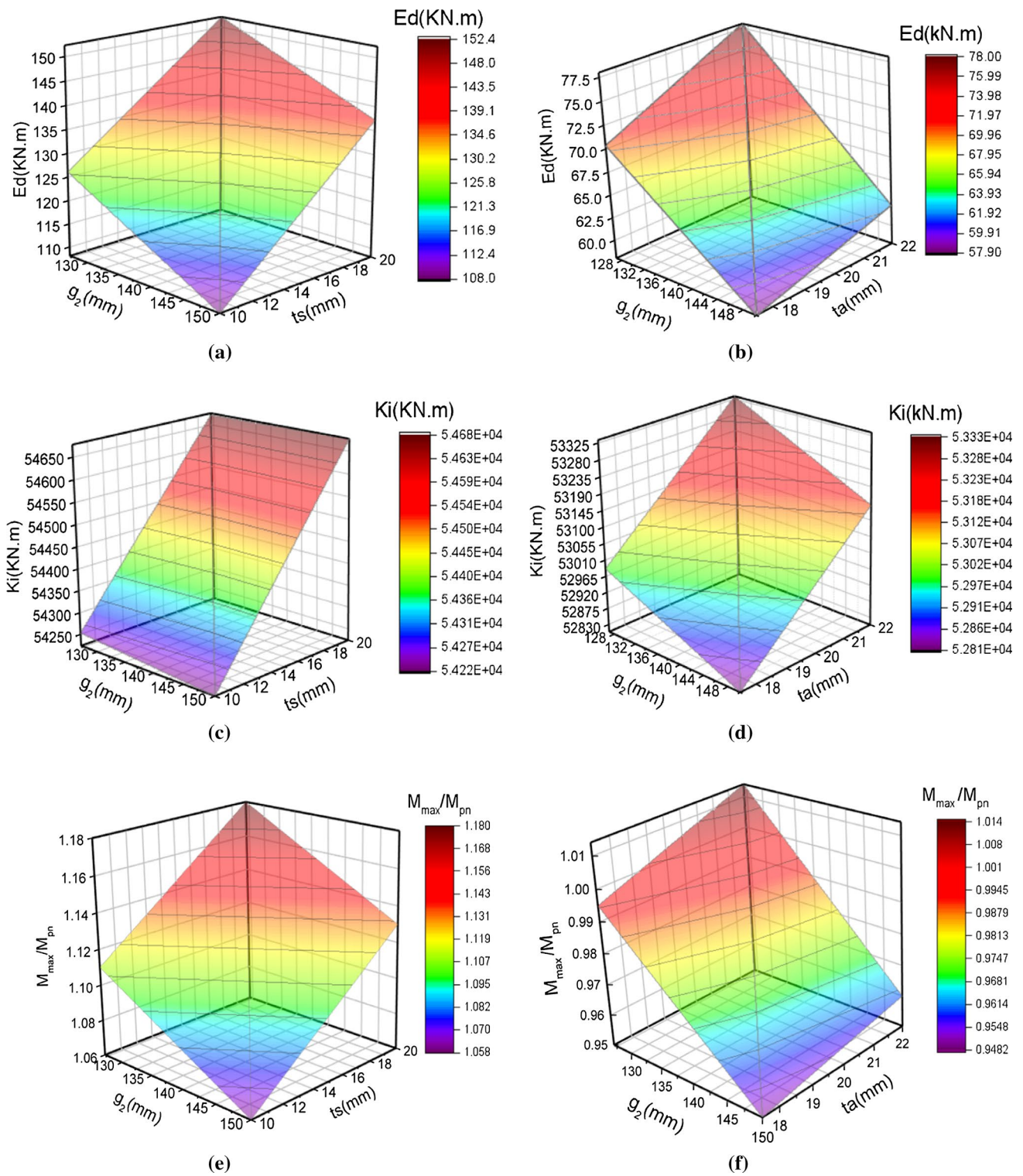


Fig. 14 (1) The simultaneous effect of t_s , g_2 on **a** energy dissipation capacity (E_d), **c** on initial stiffness (K_i), and **e** on moment capacity ($\frac{M_{max}}{M_p}$) of the PT connection.

(2) The simultaneous effect of t_a , g_2 on **b** energy dissipation capacity (E_d), **d** initial stiffness (K_i) and **f** moment capacity ($\frac{M_{max}}{M_p}$) of the PT connection

Table 7 Ratio of secant stiffness of specimens to the secant stiffness of SP02

Specimen	SP01	SP02	SP03	SP04	SP05	SP06	SP07	SP08	SP09
$\frac{K_{s_{SPn}}}{K_{s_{SP02}}}$	0.99	1	1.009	1.0178	1.008	1.0103	1.0133	1.0211	1.0341
Specimen	SP10	SP11	SP12	SP13	SP14	SP15	SP16	SP17	SP18
$\frac{K_{s_{SPn}}}{K_{s_{SP02}}}$	1.0361	1.0154	1.0207	1.0329	1.036	1.0363	1.0368	1.0355	1.0205
Specimen	SP19	SP20	SP21	SP22	SP23				
$\frac{K_{s_{SPn}}}{K_{s_{SP02}}}$	0.97	0.945	0.429	0.977	1.0124				

Table 8 Ductility of specimens

Specimen	SP01	SP02	SP03	SP04	SP05	SP06	SP07	SP08	SP09	SP10	SP11	SP12
μ	1.74	1.83	1.87	2.02	2.19	1.9	1.72	2.44	2.52	2.76	1.9	2.02
Specimen	SP13	SP14	SP15	SP16	SP17	SP18	SP19	SP20	SP21	SP22	SP23	
μ	2.29	2.67	2.58	2.52	2.22	2.08	1.68	1.53	1.3	1.59	2.3	

ity index for the PT connections with stiffeners is 2.41, which is 32% greater than that of the connection without stiffeners.

- The results show that adding the stiffeners to the angles of the PT connection improves the ductility by 32%, while a greater thickness of the angle increases the ductility up to 16%. Therefore, the effects of adding stiffener in enhancing ductility behavior of the PT connection are much greater than increasing angle thickness.

References

- ABAQUS/CAE. (2010). Version 6.11-PR3, Dassault Systems Simulia Corp., user manual, RI.
- AISC. (2016). *Specification for structural steel buildings*. Chicago, IL: American Institute of Steel Construction.
- Annan, C. D., & Chiza, A. (2013). Characterization of slip resistance of high strength bolted connections with zinc-based metallized faying surfaces. *Engineering Structures*, 56, 2187–2196.
- ASTM. (1991). Standard methods for tension testing of metallic materials. In *ASTM designation E8-91*. Philadelphia.
- ASTM. (1997). Standard specification for steel strand, uncoated seven-wired for pre stressed concrete. In *ASTM designation no. A416-94*. Philadelphia.
- Garlock, M., Ricles, J., & Sause, R. (2005). Experimental studies on full-scale post-tensioned steel connections. *Journal of Structural Engineering*, 131(3), 438–448.
- Garlock, M., Sause, R., & Ricles, J. M. (2007). Behavior and design of post-tensioned steel frame systems. *Journal of Structural Engineering*, 133(3), 389–399.
- Herning, G., Garlock, M., & Vanmarcke, E. (2011). Reliability-based evaluation of design and performance of steel self-centering moment frames. *Journal of Constructional Steel Research*, 67, 1495–1505.
- Moradi, S., & Alam, M. S. (2015). Finite element simulation of post tensioned steel connections with bolted angles under cyclic loading. *Journal of Structural Engineering ASCE*, 142(1), 04015075.
- Moradi, S., & Alam, M. S. (2017). Lateral load–drift response and limit states of post-tensioned steel beam–column connections: parametric study. *Journal of Structural Engineering ASCE*, 143, 04017044.
- Ricles, J., Sause, R., Garlock, M., & Zhao, C. (2001). Post-tensioned seismic resistant connections for steel frames. *Journal of Structural Engineering ASCE*, 127, 2113–2121.
- Ricles, J., Sause, R., Peng, S. W., & Lu, L. W. (2002). Experimental evaluation of earthquake resistant post-tensioned steel connections. *Journal of Structural Engineering ASCE*, 128(7), 850–859.
- Shiravand, M., & Mahboubi, S. (2016). Behavior of post-tensioned connections with stiffened angles under cyclic loading. *Journal of Constructional Steel Research*, 116, 183–192.
- Vasdravellis, G., Karavasilis, T. L., & Uy, B. (2013a). Finite element models and cyclic behavior of self-centering steel post-tensioned connections with web hourglass pins. *Engineering Structures*, 52, 1–16.
- Vasdravellis, G., Karavasilis, T. L., & Uy, B. (2013b). Large-scale experimental validation of steel post-tensioned connections with web hourglass pins. *Journal of Structural Engineering*, 139(6), 1033–1042.
- Venture, S. J. (1997). Protocol for fabrication, inspection, testing, and documentation of beam–column connection tests and other experimental specimens. In *Rep. no. SAC/BD-97*.
- Wolski, M., Ricles, J., & Sause, R. (2009). Experimental study of a self-centering beam–column connection with bottom flange friction device. *Journal of Structural Engineering ASCE*, 135(5), 479–488.
- Zhang, A., Zahng, Y., Li, R., & Wang, Z. (2016). Cyclic behavior of a prefabricated self-centering beam–column connection with a bolted web friction device. *Engineering Structures*, 11, 185–198.